

**CAMPBOR TREE (*Dryobalanops aromatica*) BARK  
EXTRACT AS CORROSION INHIBITOR FOR  
MILD STEEL IN ACIDIC MEDIUM**

**YAKUBU SARAYA AKUBEN**

**UNIVERSITI SAINS MALAYSIA**

**2021**

**CAMPHOR TREE (*Dryobalanops aromatica*) BARK  
EXTRACT AS CORROSION INHIBITOR FOR  
MILD STEEL IN ACIDIC MEDIUM**

by

**YAKUBU SARAYA AKUBEN**

**Thesis submitted in fulfilment of the requirements  
for the degree of  
Doctor of Philosophy**

**April 2021**

## ACKNOWLEDGEMENT

To God be the glory, honour, praise and power, the maker of heaven and earth, the source of all wisdom, knowledge and understanding, for making this PhD. journey a huge success. I would like to tender my immense gratitude to my supervisor Dr. Mohd. Hazwan Hussin for his guidance, patience, and kindness to me throughout the period of this study. He was always available for consultations and ensured that the research was continually progressive. I am deeply grateful to my co-supervisors, Prof Afidah Abdul Rahim for the insightful advice, support and contributions, and Dr. Mohammad Nurul Azmi for provision of all that was needed for my laboratory work. I appreciate the Federal Government of Nigeria for the Tertiary Education Trust Fund (TETFund) scholarship award, for my studies and Universiti Sains Malaysia for the research grant scheme 304/PKIMIA/6315100. Special thanks to Dr. Bothi Raja, Puan Siti, Puan Ami, Puan Roziana, Cik Alia, Encik Ali, Encik Azizo, administrative, and technical staff of School of Chemical Sciences, for the help I received. Also, to the technical staff of School of Physics, Industrial Technology and Archaeology Research Centre. I am grateful to my colleagues/lab mates namely, Sherwyn, Saifullahi, Majid, Hanis, Rushan, Amira, Fatin, Alif, Farah, Najahan, Shafiqah and my friends; Martha, Elom, Victoria, Edna, Marcia, Joanna, Halima and Zainab for their help and encouragements. And not forgetting my spiritual family in Excel Point Community Church Penang and Bible Study Fellowship International for being strong support for me. I will remain grateful for the prayers, supports and patience of my mother Mrs. Martha Yakubu, father-in-law Adagwom Nyam Waziri, my darling husband Mr. Yakubu Nyam Waziri and my precious daughter Ms. Kushim Yakubu Nyam, may God bless you all abundantly.

## TABLE OF CONTENTS

<b>ACKNOWLEDGEMENT</b> .....	<b>ii</b>
<b>TABLE OF CONTENTS</b> .....	<b>xvi</b>
<b>LIST OF TABLES</b> .....	<b>xxi</b>
<b>LIST OF FIGURES</b> .....	<b>xxiii</b>
<b>LIST OF SYMBOLS</b> .....	<b>xxvii</b>
<b>LIST OF APPENDICES</b> .....	<b>xxxii</b>
<b>ABSTRAK</b> .....	<b>xxxiii</b>
<b>ABSTRACT</b> .....	<b>xxxv</b>
<b>CHAPTER 1 INTRODUCTION</b> .....	<b>1</b>
1.1 Background of the study .....	1
1.2 Problem statements .....	3
1.3 Research objectives.....	4
1.4 Scope of the research .....	4
1.5 Limitation of the research .....	5
<b>CHAPTER 2 LITERATURE REVIEW</b> .....	<b>6</b>
2.1 <i>Dryobalanops aromatica</i> (Dipterocarpaceae).....	6
2.2 Tannins.....	8
2.3 Extraction and solubility of plant extract used as corrosion inhibitor .....	10
2.4 Qualitative and Quantitative analyses of plant extract inhibitor.....	11
2.5 Corrosion process.....	12
2.6 Consequences of corrosion .....	16
2.7 Economic cost of corrosion .....	17
2.8 Electrochemical corrosion monitoring techniques.....	17
2.8.1 Electrochemical impedance spectroscopy (EIS).....	18
2.8.2 Potentiodynamic polarization (PD).....	23

2.8.3	Electrochemical noise (EN) .....	28
2.9	Corrosion protection .....	31
2.10	Corrosion inhibition .....	32
2.10.1	Inhibitors .....	33
2.10.2	Types of inhibitors .....	35
2.11	Adsorption process in corrosion inhibition.....	38
2.11.1	Types of the adsorption process.....	39
2.11.2	Adsorption isotherm.....	39
2.12	Review on sol-gel coating.....	41
2.13	Review on rust converter .....	47
2.14	Surface analyses .....	49
<b>CHAPTER 3 METHODOLOGY .....</b>		<b>51</b>
3.1	Sample preparation .....	51
3.2	Chemicals and reagents.....	51
3.3	Extraction of <i>Dryobalanops aromatica</i> bark tannins.....	52
3.4	Phytochemical screening .....	54
3.5	Characterization of <i>Dryobalanops aromatica</i> bark tannin extracts.....	57
3.5.1	Fourier transformed infra-red spectroscopy (FT-IR).....	57
3.5.2	Nuclear magnetic resonance (NMR) spectroscopy.....	57
3.5.3	Thermogravimetric analysis (TGA).....	58
3.6	Quantitative analyses .....	58
3.6.1	Total phenolic content (TPC).....	58
3.6.2	Total flavonoid content (TFC).....	59
3.6.3	Total tannin content assay (TTC).....	60
3.7	Antioxidant assays .....	60
3.7.1	Reducing power .....	60
3.7.2	DPPH (2,2 -diphenyl-1-picrylhydrazyl) free radical scavenging activity.....	61

3.8	Corrosion inhibitor studies.....	62
3.8.1	Preparation of specimens .....	62
3.8.2	Preparation of electrolyte .....	62
3.8.3	Electrochemical impedance spectroscopy (EIS).....	63
3.8.4	Potentiodynamic polarization (PD).....	63
3.8.5	Electrochemical noise (EN) .....	64
3.9	Sol-gel studies .....	66
3.10	Rust phase transformation studies .....	67
3.10.1	Rust production .....	67
3.10.2	Rust treatment with extract .....	67
3.10.2(a)	Concentration study .....	67
3.10.2(b)	pH study .....	68
3.10.2(c)	Time study .....	68
3.11	Surface analyses.....	68
3.11.1	Scanning electron microscope/ energy dispersive X-ray (SEM/EDX) .....	69
3.11.2	Water contact angle.....	69
3.11.3	X-ray diffraction (XRD) .....	70
3.11.4	Summary of methodology .....	70
<b>CHAPTER 4 RESULTS AND DISCUSSION.....</b>		<b>72</b>
4.1	<i>Dryobalanops aromatica</i> bark tannin extracts (DABTEs) .....	72
4.2	Phytochemical screening of DABTEs .....	73
4.3	Characterization of DABTEs .....	76
4.3.1	Fourier transformed infra-red spectroscopy (FTIR) analysis .....	76
4.3.2	Nuclear magnetic resonance (NMR).....	77
4.3.3	Thermal gravimetric analysis (TGA).....	80
4.4	Quantitative analysis of DABTEs.....	83
4.4.1	Total phenolic content (TPC).....	83

4.4.2	Total flavonoid content (TFC) .....	84
4.4.3	Total tannin content (TTC) .....	85
4.5	Antioxidant assays .....	86
4.5.1	Reducing power assay .....	86
4.5.2	DPPH free radical scavenging assay .....	87
4.6.	Corrosion inhibition study .....	91
4.6.1	Electrochemical impedance spectroscopy (EIS).....	91
4.6.2	Potentiodynamic polarization (PD).....	100
4.6.3	Electrochemical noise .....	106
4.6.4	Effect of temperature .....	108
4.6.5	Adsorption isotherm.....	112
4.6.6	Surface analyses .....	116
4.6.7	Corrosion inhibition mechanism.....	119
4.7	Corrosion inhibition study using sol-gel coating .....	120
4.7.1	Electrochemical impedance spectroscopy (EIS).....	120
4.7.2	Potentiodynamic polarization (PD).....	130
4.7.3	Fourier transformed infra-red (FTIR) study.....	134
4.7.4	Water contact angle measurement .....	136
4.7.5	Microstructure analysis of the sol-gel coated mild steel surface .....	138
4.7.6	Sol-gel coating mechanism .....	140
4.8	Rust transformation study .....	142
4.8.1	Effect of concentration.....	144
4.8.2	Effect of pH.....	146
4.8.3	Effect of time .....	148
4.8.4	X-ray diffraction analysis .....	149
4.8.5	Mechanism of rust transformation .....	150

<b>CHAPTER 5 CONCLUSION AND FUTURE RECOMMENDATION .....</b>	<b>153</b>
5.1 Conclusion .....	153
5.2 Recommendation .....	156
<b>REFERENCES.....</b>	<b>158</b>
<b>APPENDICES</b>	
<b>LIST OF PUBLICATIONS AND CONFERENCES</b>	



## LIST OF TABLES

	<b>Page</b>
Table 2.1	Electric circuit components in electrochemical impedance ..... 20
Table 2.2	Some recent studies on plant parts as green corrosion inhibitors ..... 37
Table 2.3	Properties and significance of some adsorption isotherms ..... 40
Table 2.4	Previous studies on plant inhibitors doped hybrid sol-gel coating on a metal substrate ..... 47
Table 4.1	Extraction yield of <i>Dryobalanops aromatica</i> bark ..... 73
Table 4.2	Phytochemical screening of DABTEs ..... 75
Table 4.3	<sup>1</sup> H NMR peak assignment for DABTEs (TME and TWE)..... 78
Table 4.4	<sup>13</sup> C NMR peak assignment for DABTEs (TME and TWE)..... 79
Table 4.5	Phytochemical content of TME and TWE ..... 86
Table 4.6	Comparative EC <sub>50</sub> and ARP for antioxidant standards and DABTEs ..... 90
Table 4.7	Nyquist impedance parameters for TME inhibitor at 303 K..... 94
Table 4.8	Nyquist impedance parameters for TWE inhibitor at 303 K..... 94
Table 4.9	Electrochemical polarization parameters of mild steel in 0.5 M HCl solution without and with TME inhibitor at 303 K..... 102
Table 4.10	Electrochemical polarization parameters of mild steel in 0.5 M HCl solution without and with TWE inhibitor at 303 K..... 103
Table 4.11	Electrochemical noise parameters for optimum concentration (1000 ppm) of TME and TWE inhibitors at 303K..... 108
Table 4.12	Thermodynamic parameters for mild steel in 0.5 M HCl solution with optimum concentration (1000 ppm) of TME and TWE inhibitors ..... 109
Table 4.13	Correlation coefficient for adsorption isotherms for TME and TWE extracts inhibitors..... 114

Table 4.14	Adsorption parameters from PD measurement (inhibition study) without and with different concentrations of TME and TWE inhibitors at 30 °C ± 1 .....	116
Table 4.15	EDX elemental composition for untreated and treated mild steels in 0.5 M HCl at room temperature 30 °C ± 1 .....	118
Table 4.16	Nyquist parameters for bare, undoped and TME doped sol-gel coated mild steel of different concentrations at 303 K.....	123
Table 4.17	Nyquist parameters for bare, undoped and TWE doped sol-gel coated mild steel of different concentrations at 303 K.....	124
Table 4.18	Electrochemical polarization parameters for bare, undoped and TME inhibitor doped sol-gel coated mild steel of different concentrations at 303 K.....	132
Table 4.19	Electrochemical polarization parameters for bare, undoped and TWE inhibitor doped sol-gel coated mild steel of different concentrations at 303 K.....	133
Table 4.20	EDX elemental composition for blank, undoped and doped sol-gel coated mild steels with TME and TWE inhibitors.....	140

## LIST OF FIGURES

		<b>Page</b>
Figure 2.1	Camphor tree ( <i>Dryobalanops aromatica</i> ) (Kamariyah et al., 2012).....	6
Figure 2.2	Classification of tannin (Saxena et al., 2013) .....	9
Figure 2.3	Catechin monomer (Flavan-3-ol unit) (Adopted from Enomoto et al., 2020) .....	10
Figure 2.4	Corrosion and energy changes in steel and iron (Sahan et al., 2018).....	13
Figure 2.5	Corrosion half-cell reactions (Salunkhe and Rane, 2016).....	14
Figure 2.6	EIS potential excitation and current response (Perez, 2004) .....	20
Figure 2.7	Nyquist plots (Perez, 2004).....	21
Figure 2.8	Bode plots (Berradja, 2019) .....	21
Figure 2.9	Common electrochemical circuits used in corrosion studies (Perez, 2004) .....	23
Figure 2.10	Schematic activation free energy distribution (Perez, 2004) .....	25
Figure 2.11	Hypothetical Tafel plot (Zaki, 2006) .....	27
Figure 2.12	Pourbaix diagram for iron and alloys (Ahmad, 2006) .....	32
Figure 2.13	Classification of inhibitors (Hart, 2016). .....	34
Figure 3.1	Extraction process of Camphor ( <i>Dryobalanops aromatica</i> ) tree bark.....	53
Figure 3.2	<i>Dryobalanops aromatica</i> bark crude extracts .....	54
Figure 3.3	Summary of overall experimental work on <i>Dryobalanops aromatica</i> tree bark from extraction to application analyses .....	71
Figure 4.1	FTIR spectra of DABTEs.....	76
Figure 4.2	(a) Thermogravimetric (TG) and (b) derivative thermogravimetric (DTG) curves for TME and TWE .....	82

Figure 4.3	Reducing power plots of DABTEs and standard antioxidants .....	87
Figure 4.4	DPPH free radical scavenging antioxidant for DABTEs and standard antioxidants .....	89
Figure 4.5	Nyquist impedance plots for mild steel in 0.5 M HCl solution with different concentrations of TME at 303 K .....	92
Figure 4.6	Nyquist impedance plots for mild steel in 0.5 M HCl solution with different concentrations of TWE at 303 K.....	92
Figure 4.7	Proposed Randle's equivalent electric circuit for bare mild steel in 0.5 M HCl at 303 K.....	94
Figure 4.8	Bode plots (a) Bode impedance magnitude (b) phase angle plots for mild steel in 0.5 M HCl solution without and with different concentrations of TME inhibitor at 303K .....	98
Figure 4.9	Bode plots (a) Bode impedance magnitude (b) phase angle plots for mild steel in 0.5 M HCl solution without and with different concentrations of TWE at 303 K.....	99
Figure 4.10	Tafel plots for hybrid sol-gel coatings in 0.5 M HCl solution with various concentrations of TME at 303 K .....	100
Figure 4.11	Tafel plots for hybrid sol-gel coatings in 0.5 M HCl solution with various concentrations of TWE at 303 K.....	101
Figure 4.12	Electrochemical current noise spectra after 1hr immersion in 0.5M HCl at 303 K.....	106
Figure 4.13:	Electrochemical potential noise spectra after 1h immersion in 0.5 M HCl at 303 K.....	107
Figure 4.14	Arrhenius plot of CR against 1/T for TME and TWE at optimum concentration of 1000 ppm .....	109
Figure 4.15	Modified Arrhenius plot of CR/T against 1/T for TME and TWE at optimum concentration of 1000 ppm.....	111
Figure 4.16	Langmuir adsorption isotherm from PD measurement using different concentrations of TME inhibitor at 303 K.....	113
Figure 4.17	Langmuir adsorption isotherm from PD measurement using different concentrations of TWE inhibitor at 303 K .....	114
Figure 4.18	SEM micrographs for (a) polished bare mild steel (b) acid treated mild steel (blank) (c) 1000 ppm TME inhibitor treated mild steel (d) 1000 ppm TWE inhibitor treated mild steel at 500x magnification after 24 h immersion in 0.5 M HCl .....	117

Figure 4.19	Proposed schematic corrosion inhibition mechanism of the adsorption of tannin molecule (from DABTEs) on to mild steel surface (Adopted from Goyal et al. 2018) .....	120
Figure 4.20	Nyquist plot for mild steel in 0.5 M HCl at 303 K, coated with hybrid sol-gel undoped and doped with TME .....	121
Figure 4.21	Nyquist plots for mild steel in 0.5 M HCl at 303 K, coated with hybrid sol-gel undoped and doped with TWE .....	121
Figure 4.22	Proposed equivalent electric circuits used to fit EIS data for (a) bare mild steel (b) hybrid sol-gel coated mild steel in the absence and presence of TME and TWE in 0.5 M HCl at 303 K .....	122
Figure 4.23	Bode impedance diagrams: (a) Bode modulus plots (b) Bode phase angle plots for mild steel in 0.5 M HCl solution with different concentrations of TME doped hybrid sol-gel coatings .....	128
Figure 4.24	Bode impedance diagrams: (a) Bode modulus plots (b) Bode phase angle plots for mild steel in 0.5 M HCl solution with different concentrations of TWE doped hybrid sol-gel coatings .....	129
Figure 4.25	Tafel plots for hybrid sol-gel coated mild steel in 0.5 M HCl solution undoped and doped with various concentrations of TME inhibitor.....	131
Figure 4.26	Tafel plots for hybrid sol-gel coated mild steel in 0.5 M HCl solution undoped and doped with various concentrations of TWE inhibitor .....	131
Figure 4.27	FTIR spectra for hybrid sol-gel coating, hybrid sol-gel coating doped with TME inhibitor and hybrid sol-gel coating doped with TWE inhibitor.....	135
Figure 4.28	Images of water contact angle of (a) bare mild steel (b) hybrid neat sol-gel coated mild steel (c) hybrid sol-gel coating doped with 1000 ppm TME inhibitor (d) hybrid sol-gel coating doped with 1000 ppm TWE inhibitor.....	137
Figure 4.29	SEM micrographs of mild steel after 24 h immersion in 0.5 M HCl solution for (a) blank mild steel (uncoated) (b) hybrid neat sol-gel coated mild steel (c) hybrid sol-gel coated mild steel with 1000 ppm TME inhibitor (d) hybrid sol-gel coated mild steel with 1000 ppm TWE inhibitor .....	139
Figure 4.30	Proposed schematic mechanism of inhibitor doped hybrid sol-gel coating on mild steel substrate .....	142

Figure 4.31	Comparative FTIR spectra of salt spray generated rust and rust standards.....	144
Figure 4.32	FTIR spectra for untreated and treated rust powder with various concentrations of TME rust converter at various concentrations .....	146
Figure 4.33	FTIR spectra for untreated and treated rust powder with 6 % TME rust converter at various pH .....	147
Figure 4.34	FTIR spectra for untreated and treated rust powder with 6 % TME rust converter at pH 4 at various period .....	148
Figure 4.35	XRD spectra for untreated and treated rust powder with 6 % TME at pH for 1 day .....	150
Figure 4.36	Proposed rust transformation mechanism of the reaction between TME rust converter and mild steel rust powder with 6 % TME, pH 4 after 1day (Adopted from Abdulmajid et al. 2019).....	152

## LIST OF SYMBOLS

A	Exposed surface area
$A$	Absorbance
$\alpha$	Symmetry coefficient
$\alpha$ -FeOOH	Goethite
B	Stern-Geary coefficient
$\beta_a$	Anodic Tafel slope
$\beta_c$	Cathodic Tafel slope
$\beta$ -FeOOH	Akaganite
C	Concentration
$C$	Capacitance
$C_{dl}$	Double layer capacitance
d	Coating thickness
$\rho$	Density
$\sigma$	Standard deviation
$\sigma_i$	Standard deviation of current
$\sigma_v$	Standard deviation of potential
E	Applied potential
$\varepsilon$	Dielectric constant
$\varepsilon_o$	Electric permittivity
$E_a$	Activation energy
$E_{corr}$	Corrosion potential
$E_o$	Open circuit potential
F	Faraday
f	Frequency
$f$	Molecular interaction parameter
Fe <sub>3</sub> O <sub>4</sub>	Magnetite
G	Goethite

$\Delta G^\circ$	Free Gibb's energy
$\gamma_a$	Chemical reaction constant
$\gamma\text{-FeOOH}$	Lepidocrocite
$h$	Planck's constant
$\Delta H$	Enthalpy change
HCl	Hydrochloric acid
$i$	Current density
$i_{\text{corr}}$	Corrosion current density
I	Current
$i_r$	Reverse current density
$i_f$	Forward current density
K	Kelvin
$K$	Equilibrium constant
$K_{\text{ads}}$	Strength of adsorption
$k'_f$	Forward reaction rate constant
$k'_r$	Reverse reaction rate constant
$L$	Inductance
$\ell$	Peak intensity
M	Magnetite
$M$	Molar
$m$	Coating surface roughness
$M_{\text{eq}}$	Equivalent weight of metal
N	Avogadro's number
$n$	Metal surface roughness
$\eta$	Overpotential
$\eta_a$	Anodic overpotential
$\eta_c$	Cathodic overpotential



NaCl	Sodium chloride
R	Gas constant
$R$	Resistance
$R_A$	Arrhenius rate of reaction
$r$	Roughness factor
$R_{ct}$	Charge transfer resistance
$R_{coat}$	Coating resistance
$R_F$	Faraday rate of reaction
$R_n$	Noise resistance
$R_p$	Polarization resistance
$R_s$	Solution resistance
$\Delta S$	Entropy change
T	Transmittance
$T$	Temperature
$\theta$	Phase angle
$\theta_w$	Water contact angle
$\omega$	Angular frequency
$Y_o$	Magnitude of CPE
$z$	Oxidation number
Z	Impedance
$Z_D$	Diffusion impedance

## LIST OF ABBREVIATIONS

AA	Ascorbic acid
AC	Alternating current
AEAPS	N-(2-amino ethyl) 3-aminopropyltrimethoxysilane
APTES	Aminopropyltriethoxysilane
APTMS	3-aminopropyltrimethoxysilane
ARP	Antiradical power
BHT	Butylated hydroxytoluene
CCC	Chromate conversion coating
CE	Counter electrode
CEQ	Catechin equivalence
CT	Catechin
DABTEs	<i>Dryobalanops aromatica</i> bark tannin extracts
DC	Direct current
DPPH	2,2-diphenyl-1-picrylhydrazyl
DTG	Derivative of thermogravimetric analysis
EC <sub>50</sub>	Effective concentration at 50 %
EDX	Electron diffraction X-ray
EIS	Electrochemical impedance spectroscopy
EN	Electrochemical noise
F-C	Folin-Ciocalteu
FTIR	Fourier transformed infra-red
GA	Gallic acid
GAE	Gallic acid equivalence
GPTMS	3-glycidoxypropyltrimethoxysilane
IE	Inhibition efficiency
IUCN	International union for conservation of nature
MAPTS	3-methacryloxypropyltrimethoxysilane

MTES	Methyltriethoxysilane
MTMS	Methyltrimethoxysilane
NACE	National Association of Corrosion Engineers
NMR	Nuclear magnetic resonance
OCP	Open circuit potential
<i>PC</i>	Procyanidin
PD	Potentiodynamic polarization
<i>PD</i>	Prodelphinidin
PTMS	Phenyltrimethoxysilane
RE	Reference electrode
SCE	Saturated calomel electrode
SEM	Scanning electron microscope
TEOS	Tetraethoxysilane
TFC	Total flavonoid content
TGA	Thermogravimetric analysis
TME	Tannin methanol extract
TPC	Total phenolic content
TTC	Total tannin content
TWE	Tannin water content
UV-vis	Ultra-violet visible spectrophotometry
XRD	X-ray diffraction
ZRA	Zero resistance ammeter

## LIST OF APPENDICES

Appendix 1a	$^1\text{H}$ NMR for TME
Appendix 1b	$^1\text{H}$ NMR for TWE
Appendix 2a	$^{13}\text{C}$ NMR for TME
Appendix 2b	$^{13}\text{C}$ NMR for TWE
Appendix 3	Gallic acid standard calibration graph for TPC
Appendix 4	Catechin standard calibration graph for TFC
Appendix 5a	Freundlich adsorption isotherm for TME
Appendix 5b	Freundlich adsorption isotherm for TWE
Appendix 6a	Temkin adsorption isotherm for TME
Appendix 6b	Temkin adsorption isotherm for TWE
Appendix 7a	El-awady adsorption isotherm for TME
Appendix 7b	El-awady adsorption isotherm for TWE
Appendix 8	EDX spectra for corrosion inhibition study
Appendix 9	EDX spectra for hybrid sol-gel coating study

**EKSTRAK KULIT POKOK KAPUR BARUS (*Dryobalanops aromatica*)  
SEBAGAI PERENCAT KAKISAN BAGI KELULI LEMBUT DALAM  
LARUTAN BERASID**

**ABSTRAK**

Matlamat kajian ini adalah untuk mengekstrak tanin daripada kulit pokok kapur barus (*Dryobalanops aromatica*) dan mengkaji keupayaan perlindungan kakisan daripada ekstrak tanin pada keluli lembut dalam larutan 0.5 M HCl. Pengekstrakan dilakukan melalui kaedah rendaman dan memberikan peratusan hasil secara tertib ekstrak metanol > ekstrak air > ekstrak etil asetat > ekstrak heksena. Ekstrak methanol tanin (TME) dan ekstrak air tanin (TWE) dicirikan secara kualitatif dan kuantitatif. Spektra spektroskopi infra merah Fourier (FTIR) menunjukkan kehadiran kumpulan berfungsi yang mencirikan sifat perencat kakisan. Resonans magnetik nuklear karbon-13 tanin (<sup>13</sup>C NMR) menunjukkan bahawa kedua-dua TME dan TWE mempunyai signal karbon-13 bagi prosianidin tanin. Jumlah kandungan fenolik (TPC) ditentukan dengan kaedah Folin-Ciocalteau, jumlah kandungan flavonoid (TFC) melalui kaedah kolorimetri aluminium klorida dan jumlah kandungan tanin (TTC) dengan kaedah Stiasny didapati lebih tinggi pada TME daripada TWE. Ujian antioksidasi mendapati bahawa kuasa penurunan dan kapasiti pemulungan radikal bebas adalah lebih kuat pada TME berbanding dengan TWE. Kajian perencatan kakisan yang dilakukan dengan menggunakan teknik spektroskopi impedans elektrokimia (EIS), potensidynamik (PD) dan hingar elektrokimia (EN) mendapati bahawa kecekapan perencatan (IE) TME dan TWE meningkat dengan kepekatan hingga 1000 ppm dan kecekapan perencatan menggunakan tiga teknik berbeza adalah dalam julat 80 - 93 % bagi TME dan 80 - 92 % bagi TWE. Kesemua data eksperimen dipadankan dengan

isoterm penjerapan Langmuir, mekanisma penjerapan fizikal menerangkan proses perencatan. Penglitup sol-gel hibrid (GPTMS-TEOS) yang didopkan dengan TME dan TWE menunjukkan peningkatan perlindungan keluli lembut dengan IE sedikit tinggi ( $IE_{TME} = 93.68 \%$ ,  $IE_{TWE} = 93.64 \%$ ) berbanding dengan penglitup sol-gel hibrid tanpa dopan (53.66 %). Penglitupan keluli lembut dengan sol-gel didopkan TME memberikan sifat hidrofobik yang baik dengan sudut sentuhan air  $122.73^\circ$  berbanding dengan keluli lembut terlitup sol-gel hibrid didopkan TWE dengan sudut sentuhan air  $88.68^\circ$ . Tambahan pula, lebih dari 90% transformasi kepada ferik tanat telah berjaya dicapai pada keadaan optimum 6 % TME pada pH 4 selama 1 hari. Pembentukan ferik tanat telah ditentukan menggunakan analisis FTIR dan pembelauan sinar-X. Oleh yang demikian, TME telah terbukti sebagai perencat terbaik berbanding TWE bagi keluli lembut dalam 0.5 M HCl daripada kajian perencat kakisan, penglitup sol-gel hibrid serta berpotensi sebagai pengubah karat.

**CAMPHOR TREE (*Dryobalanops aromatica*) BARK EXTRACT AS  
CORROSION INHIBITOR FOR MILD STEEL IN ACIDIC MEDIUM**

**ABSTRACT**

The goal of the study is to extract tannin from the bark of camphor tree (*Dryobalanops aromatica*) and to study the corrosion inhibition potential of the tannin extracts on mild steel in 0.5 M HCl. The extraction was carried out through maceration, gave percentage yield in the order of methanol extract > water extract > ethyl acetate extract > hexane extract. The tannin methanol extract (TME) and tannin water extract (TWE) further characterized qualitatively and quantitatively. The Fourier transformed infrared spectroscopy (FTIR) spectra for both extracts revealed the presence of functional groups that characterise good corrosion inhibitor. The carbon-13 nuclear magnetic resonance (<sup>13</sup>C NMR) showed that both TME and TWE contain carbon-13 signals for procyanidin tannin. The total phenolic content (TPC) carried out by Folin-Ciocalteu method, total flavonoid content (TFC) by aluminium chloride colorimetric method, total tannin content (TTC) assay by Stiasny method were found to be higher in TME than TWE. The antioxidant assays revealed that TME has more reducing and antiradical power than TWE. The results from the corrosion inhibition studies conducted via electrochemical impedance spectroscopy (EIS), potentiodynamic polarization (PD) and electrochemical noise (EN) techniques showed that, inhibition efficiencies (IE) of TME and TWE increased with concentration up to 1000 ppm and the IE from the three different techniques were within the range of 80 - 93 % for TME and 80 - 92 % for TWE. All the experimental data for both tannin extracts fitted best into the Langmuir adsorption isotherm and physisorption mechanism described the inhibition process. The hybrid sol-gel coating (GPTMS-TEOS) doped with TME and

TWE revealed greater enhancement protection of the mild steel, having higher IE ( $I.E_{TME} = 93.68\%$ ,  $I.E_{TWE} = 93.64\%$ ) than the undoped hybrid sol-gel coating (53.66 %). The TME doped hybrid sol-gel coated mild steel exhibited better hydrophobic property with contact angle of  $122.73^\circ$  than TWE doped hybrid sol-gel coated mild steel with contact angle of  $88.68^\circ$ . Additionally, more than 90 % rust transformation into ferric tannates was achieved with 6 % TME at pH 4 and after 1 day. The formation of ferric tannates was confirmed by FTIR and X-ray diffraction (XRD) analyses. Therefore, TME has proven to be a better inhibitor than TWE for mild steel in 0.5 M HCl from the corrosion inhibition and hybrid sol-gel coating studies, as well as a potential rust converter.



# CHAPTER 1

## INTRODUCTION

### 1.1 Background of the study

As an engineering tool, mild steel or carbon steel remains the backbone for a spectrum of industries such as automobile, aviation, automotive, building, construction, machinery, transportation, oil, and gas (Shainy et al., 2016). Mild steel has become a valuable material for most industrial processes and manufacturing due to its ease of availability, low cost and outstanding mechanical properties (Saeed et al., 2020). In the petroleum industry, the use of acids in industrial cleaning, acid pickling and acid descaling create an aggressive environment leading to the corrosion of mild steel (Finšgar and Jackson, 2014). Moreover, due to the less amount of alloy, mild steel is prone to high corrosion with not more than 2 per cent carbon of its total weight (Qian et al., 2009).

One of the most feasible corrosion mitigation methods, especially in acidic media, is the use of inhibitors (Anupama et al., 2016). Although available conventional synthetic organic inhibitors have proven to be very effective, they are to some degree, toxic and very expensive. The recent strict environmental legislation and increasing awareness among scientists on the hazard of such inhibitors to both humans and the environment have shifted the focus of modern researchers, to the development of “green” alternatives to mitigate corrosion (Bourazmi et al., 2018).

The use of sol-gel coating can serve as a replacement for phosphating and chromating treatments. Although these coating applications are simple and inexpensive, they are possible contaminants of soil and groundwater, and chromium

(VI) species is considered to be highly toxic in nature and carcinogenic (Qian et al., 2009). Sol-gel coatings are usually thin and porous, which lower their mechanical integrity. To achieve a dense microstructure at high sintering temperature, sol-gel coatings develop cracks due to thermal expansion coefficients and potential chemical reactions at the interface. Synthesizing hybrid coating is the key to obtaining dense sol-gel coating. And by incorporating inhibitors, the micropores are sealed to prevent corrosion species such as  $\text{Cl}^-$ ,  $\text{H}_2\text{O}$  and  $\text{O}_2$  from reaching the mild steel surface.

The most significant form of corrosion in iron and alloys is rust, which is typically unavoidable. The traditional techniques for rust removal, such as sandblasting, require a lot of energy and equally time-consuming (Nasrazadani, 1997). Therefore, the use of rust converter has become essential for corrosion mitigation (Collazo et al., 2010a). Corrosion inhibitors that are rich in polyphenolic compounds such as tannins have been considered as excellent rust converters because they can convert active rust to harmless adherent protective compounds on which overcoat painting is feasible (Merino et al., 2017). This occurs when the hydroxyl groups of the aromatic rings of the tannin molecules react with ferric ions to form highly crosslinked network of blue-black ferric tannate, which forms a passivation against further corrosion (Mei et al., 2015).

*Dryobalanops* is a unique genus of Dipterocarpaceae plant as only seven species exist worldwide, namely, *Dryobalanops aromatica*, *Dryobalanops oblongifolia*, *Dryobalanops lanceolata*, *Dryobalanops beccarii*, *Dryobalanops rappa*, *Dryobalanops keithii*, and *Dryobalanops fusca* (Harada et al., 2018; Dwiyantri et al., 2015). Most of these species are found in tropic regions of Peninsular Malaysia, Sumatra, and Borneo (Rachmayanti et al., 2006). The trees of Dipterocarpaceae are distinct and well-known in the tropics as they stand tall in some of the earth's majestic

forest formation (Juliana et al., 2018). Their overwhelming presence led to them being referred to as dipterocarp forests. A group of large trees of these species forms a high uniform canopy that gives rise to structural differences compared to other dipterocarp forest types (Norafida et al., 2018).

## 1.2 Problem statements

The problem of corrosion is like “cancer” to steel since it cannot be totally eliminated, but can only be minimized or managed (Fan and Zhao, 2011). Unfortunately, the most effective corrosion inhibitors with long standing history are extremely toxic and very expensive. The use of inorganic inhibitors such as red lead and zinc chromate have been regulated by law, due to their carcinogenicity on humans and harmful potential to the environment.

The use of hybrid sol-gel coating on metal substrates also provide protection against corrosion attack. However, the coating may be characterized by some micropores and microcracks through which aggressive corrosion agents could get to the surface of the substrate been protected thereby, rendering the coating ineffective. Likewise, rust converters which act by converting active rust substance to protective compounds are mostly synthesized with hazardous and unsafe chemicals which are environmentally unfriendly.

Due to the popular demand for the wood of camphor tree, the bark constitutes a huge agricultural waste after the trees are logged (Ritonga et al., 2018). Additionally, the continuous falling of the trees to make way for oil palm plantation poses serious threat to *Dryobalanops aromatica* species. According to Kuspradini et al. 2007, *Dryobalanops aromatica* tree bark contains tannin. Tannins possess heteroatoms with

lone pairs of electrons, pi-electrons of aromatic rings and phenolic hydroxyl groups that confer the ability to inhibit corrosion (Gambier et al., 2018).

### **1.3 Research objectives**

The goal of this study is to explore the suitability of *Dryobalanops aromatica* bark tannin extracts as a green inhibitor for mild steel in acidic medium, to provide a safer alternative for toxic inorganic inhibitors and costly synthetic organic inhibitors, that are widely used in industrial processes. After the extraction and characterization of the bark extracts, the work was set to achieve the following objectives:

1. To explore the potential of *Dryobalanops aromatica* bark tannin extracts as green inhibitor of mild steel corrosion in hydrochloric medium, using electrochemical techniques, surface analyses and, to propose possible mechanism.
2. To evaluate the efficacy of incorporating *Dryobalanops aromatica* bark tannin extract in hybrid sol-gel coating for mild steel corrosion protection through electrochemical technique, surface analyses and, to propose the possible mechanism.
3. To ascertain the potential of *Dryobalanops aromatica* bark tannin extract in rust transformation by varying the reaction conditions (Concentration, pH, and time) and, to propose the possible mechanism.

### **1.4 Scope of the research**

This research work includes studying the dried bark of *Dryobalanops aromatica* collected from Kepong Selangor as a possible green inhibitor for mild steel corrosion. The crude plant extracts obtained by maceration were qualitatively and

quantitatively characterized before been used in three (3) application studies. Firstly, inhibition study in 0.5 M HCl medium by varying concentrations (10 ppm – 1000 ppm) and temperatures (303 K – 333 K) to achieve best conditions for the inhibition. Secondly, sol-gel coating study by varying the mixing ratios (1:1, 1:2, 1:3, 2:1, 3:1) of precursors to obtain the most appropriate mixture. The different concentrations of inhibitor as in the inhibition study (50 ppm – 1000 ppm) was doped to the hybrid sol-gel coating deposited on mild steel. Thirdly, rust converter study which involves treatment of salt spray produced rust at varying concentrations (0.5 % - 8 %), pH (2 – 8), and contact time (1/2 – 14 days), to obtain the best conditions of the rust transformation. Following these three application studies, the mild steels from the first two studies were characterized by electrochemical measurements (Electrochemical impedance spectroscopy, Potentiodynamic polarization and Electrochemical noise techniques), and surface analyses (Scanning electron microscope, Energy disperse X-ray and water contact angle measurement). While the rust powder (treated and untreated) from the last study was characterized by Fourier transformed spectroscopy and X-ray diffraction. The mechanisms for each of these three studies were then proposed.

## **1.5 Limitation of the research**

The Electrochemical noise analysis could not be carried out for hybrid sol-gel coating application study due to the breakdown of the potentiostat as at the time of the study.

## CHAPTER 2

### LITERATURE REVIEW

#### 2.1 *Dryobalanops aromatica* (Dipterocarpaceae)



Figure 2.1: Camphor tree (*Dryobalanops aromatica*) (Kamariyah et al., 2012)

Camphor tree is a woody plant that grows up to 70 meters tall when fully matured and spreads widely across these dipterocarp forests (Yahya and Gardingen, 1999; Kamariyah et al., 2012). Other names of the tree with regards to geographical

location are Sumatra camphor, Malay camphor, and Borneo camphor tree. The species name “*aromatica*” refers to the fragrant smell of a white resinous substance (the “true camphor”), which is released from the different parts of the tree. *Dryobalanops aromatica* is essentially outbreeding and pollinated by insects. Due to its winged fruits, the seeds are dispersed by gravity or gyration (Harada et al., 2018). The stem is a good source of camphor oil (camphor essential oil), which finds application in oral and topical medications (Kamariyah et al., 2012). The oil of camphor tree has been reported with various biological activities, including antioxidant properties, anti-cancer and anti-HIV (Le et al., 2016).

The tree of *Dryobalanops aromatica* is famous for its high-quality timber with trade name “kapur”, which predominated the international tropical wood market and played a vital role in many Southeast Asian countries (Appanah et al., 1998). The wood is usually used for heavy construction purposes and, in the past, was used as rail sleepers. The exciting feature of *Dryobalanops aromatica* is the peeling of its flaky bark from the trunk, which sometimes resembles a scroll of papers used to weave baskets and make walls of huts by surrounding dwellers in olden days (Corlett and Primack, 2005). Nowadays, after *Dryobalanops aromatica* trees are harvested in the forest to make timbers, piles of the trees’ bark are left wasted. The tree of *Dryobalanops aromatica* has been classified as endangered in the 2017 IUCN red list of threatened species of dipterocarp forests (Rachmayanti et al., 2006), where Malaysia is a member of IUCN. Over the years, there is an increase in human activities of incessant logging of the trees for construction purposes as well as the forests conversion into oil palm plantations for commercial purposes (Susilowati et al., 2018). These expose *Dryobalanops aromatica* species to the risk of complete extinction, with very few of the sub-population remaining in forest reserve (Ritonga et al., 2018).

Only a few information is available on the potentials of the tree of *Dryobalanops aromatica*. Most of the chemical constituents isolated were from the bark of the plant. The bark of *Dryobalanops aromatica* was previously reported to contain terpenoid and flavonoid (Bate-Smith and Whitmore, 1959), steroid and saponin (Carrick et al., 1968). The triterpenes from the resin of the bark of *Dryobalanops aromatica* tree have been characterized (Cheung and Wong, 1972; Le et al., 2017). Wibowo et al. (2012) and Manshoor et al. (2015) have reported the isolation and characterization of some oligostilbenes from the bark of *Dryobalanops aromatica*. These are complex polyphenolic compounds known as resveratrol (4,3,5'-trihydroxystilbenes) oligomers, with excellent antioxidant activity (Wang and Yao, 2016). According to Kuspradini et al. 2007, the phenolic compounds of *Dryobalanops aromatica* bark extract constitutes tannins, mainly ellagitannins; therefore, they could be a potential inhibitor for corrosion protection.

## **2.2 Tannins**

Tannins are polyphenolic secondary metabolites of higher plants, widely distributed in many plant species and found in wood, bark, leaves, seeds, and fruits. They are derivatives of galloyl ester, in which their galloyl moieties are attached to a core centre made of catechin, polyol or triterpenoid (Abdulmajid et al., 2019). Based on their structural and chemical properties, tannins can be divided into four (4) significant classes; Gallo tannins, ellagitannins, complex tannins, and condensed tannins as given in Figure 2.2.



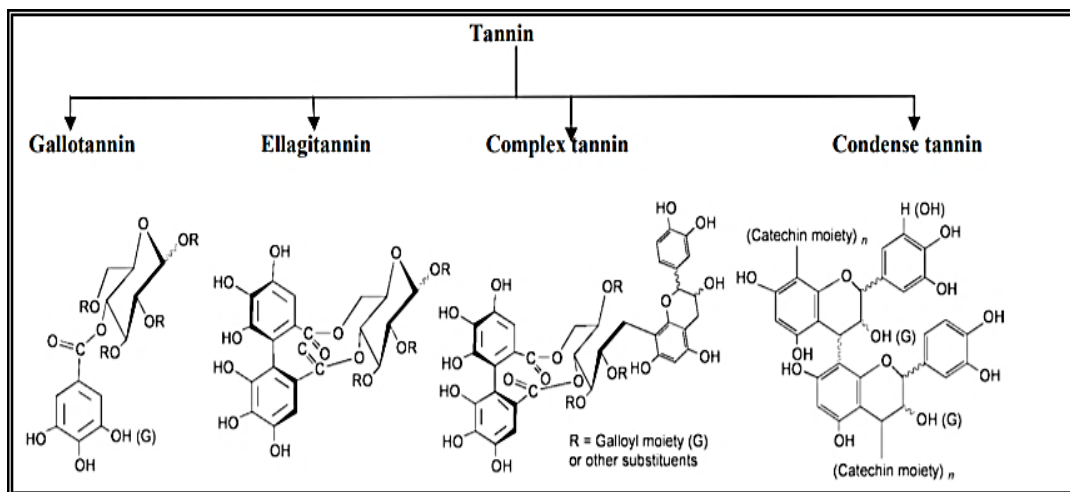


Figure 2.2: Classification of tannin (Saxena et al., 2013)

- (i) Gallotannins are tannins in which different catechin, polyols, or triterpenoid units are bonded to galloyl units or their derivatives.
- (ii) Tannins with two galloyl units bound to each other by C-C bonds are ellagitannins and do not contain a glycosidic catechin bonding unit.
- (iii) Ellagitannin and gallotannin units that are glycosidically bonded to a catechin form complex tannins.
- (iv) Condensed tannins are oligomeric and polymeric proanthocyanidins formed by coupling one catechin monomer to C-4 and another catechin monomer to C-8 or C-6.

The basic structure of condensed tannins is based on the repeating units of flavonoid, primarily flavan-3-ol repeating units (Figure 2.3), whose derivatives are namely: (+)-catechin, (-)-epicatechin, (+)-gallocatechin, (-)-epigallocatechin and (-)-epigallocatechin gallate (Koleckar et al., 2008).

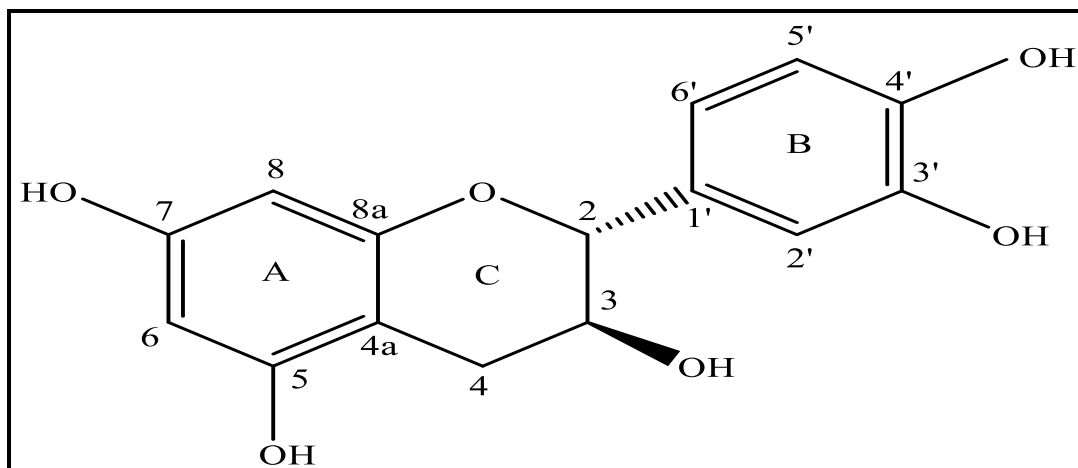


Figure 2.3: Catechin monomer (Flavan-3-ol unit) (Adopted from Enomoto et al., 2020)

Condensed tannins are found in a substantial amount in the wood and bark of several trees, such as black wattle, melaleuca, acacia, larch, oak, pine, and mangrove. Extensive research on tannins has led to a broad range of industrial applications being developed. These include use in tanneries, wood adhesives, manufacture of inks, dyeing of textiles, flocculant for water treatment, dispersants, antioxidants, corrosion inhibitors, rust converters, and so on (Pizzi, 2019).

The development of corrosion inhibitors from waste materials is sustainable, as they are being recycled instead of discarded. Plant wastes such as bark, fruit, peels, seeds have high antioxidant properties and are rich in phytochemicals which can be solvent-extracted and use as corrosion inhibitor.

### 2.3 Extraction and solubility of plant extract used as corrosion inhibitor

Extraction method greatly influences the composition of plants extracts (Arbenz and Avérous, 2015). The phytochemical constituents such as tannins, flavonoid, saponins and other polyphenolic compounds involved in corrosion inhibition can be extracted from either fresh or dried plant material (Miralrio and

Vázquez, 2020). One of the common traditional methods of extraction, that is simple, easy, and affordable is maceration (Uysal et al., 2019). In maceration, cut, crushed, or powdered plant material is immersed in a selected extraction solvent, inside a stoppered container for a period of at least three (3) days under constant agitation, at room temperature (Nn, 2015). The solvent also plays a key role in the extraction method, since it is responsible for the solubilizing of the compounds when it diffuses through the plant tissues, making their extraction possible (Miralrio and Vázquez, 2020). Extraction solvents have shown to affect the physical, chemical and antioxidant properties of extracts that are obtained. Therefore, various solvents including polar (water and alcohols), intermediate (ethyl acetate) and non-polar (hexane) are used to achieve the desired concentration of the phytochemicals of the plant extract. The solvent is separated from the mixture by decanting, filtering, and vacuum evaporating. The concentrated dried crude extract is obtained preferably by freeze drying, which is the best method for preserving the structure of the phenolic compounds and the molar masses of condensed tannin (Arbenz and Avérous, 2015).

#### **2.4 Qualitative and Quantitative analyses of plant extract inhibitor**

Qualitative analysis is carried on the plant extract to test for the presence of phytochemicals, usually the polyphenolic compounds that possess hydroxyl groups and heteroatoms such as O, N, S, P, which are required to be present for the inhibition process to take place. These compounds include tannin, flavonoid, saponin, terpenoid, glycoside and coumarin. The analysis is mostly carried out using solutions of salts and acids. For instance, ferric chloride solution used to test for the presence of tannin. An indication of positive test is usually observed by colour change of the reaction solution or precipitate formed.

Quantitative measurements are carried out to check the amount of phytochemical constituent in a plant extract. Some of the common measurements include total phenolic content (TPC), total flavonoid content (TFC) and total tannin content (TTC). In most cases, the analysis involves addition of certain reagents, salt, and acid solutions. The use of a standard compound is sometimes required. After developing the colour of both the standard and sample solutions (incubation), the solutions are then measured spectrophotometrically. A standard calibration graph is obtained for the standard solution at various concentration, and concentration of the sample is calculated. For instance, measurement of TPC with gallic acid standard using Folin-Ciocalteu reagent and  $\text{Na}_2\text{CO}_3$  salt solution. The Prussian blue colour of the solutions is measured at 765 nm using UV-VIS spectroscopy.

## **2.5 Corrosion process**

The term corrosion was derived from the Latin word '*corrodere*' which means "to gnaw to pieces" (Davis, 2000). Corrosion is usually the degradation through chemical reaction of materials such as metals, plastics, ceramics, polymers, cement, and wood, with their surrounding environment (Landolt, 2007). Nevertheless, in most cases, the term corrosion refers to metals' destructive attack by chemical or electrochemical reaction with the environment (Zaki, 2006). All metals are usually found in nature as ores, but during manufacturing processes with energy input, these ores are converted into pure metals, as illustrated in Figure 2.4. However, when corrosion occurs, the added energy is released, and the metal returned to its original oxide state in which is thermodynamically stable.

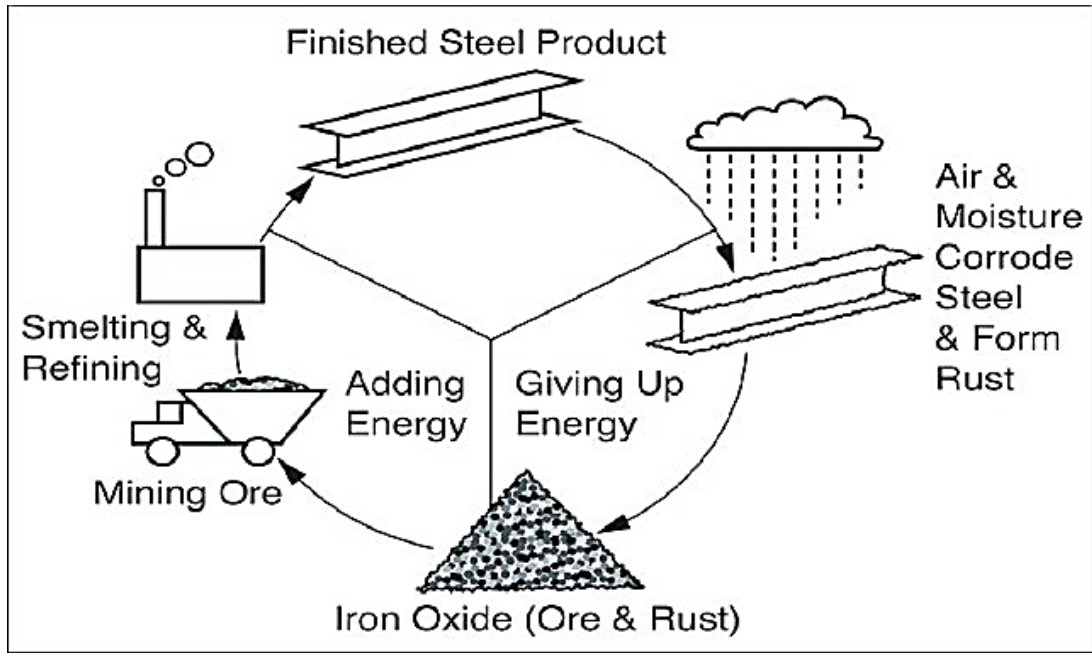


Figure 2.4: Corrosion and energy changes in steel and iron (Sahan et al., 2018)

Corrosion in an aqueous medium is an electrochemical process. In a corroding device (Bradford and Bradford 1993), the following components are required: the anode (the metal corroding); the cathode (a metal or other electronic conductors whose surface becomes reaction sites for the medium); and the electrolyte (the aqueous environment which provides an ionic link path between the anode and the cathode). The absence of any one of these components will imply that the electrochemical corrosion will not occur. Thus, analysis of the corrosion cell may provide a hint on how to stop the corrosion process. Two half-cell reactions, the anode reaction, and the cathode reaction, as illustrated in Figure 2.5, are involved in the iron or steel corrosion process.

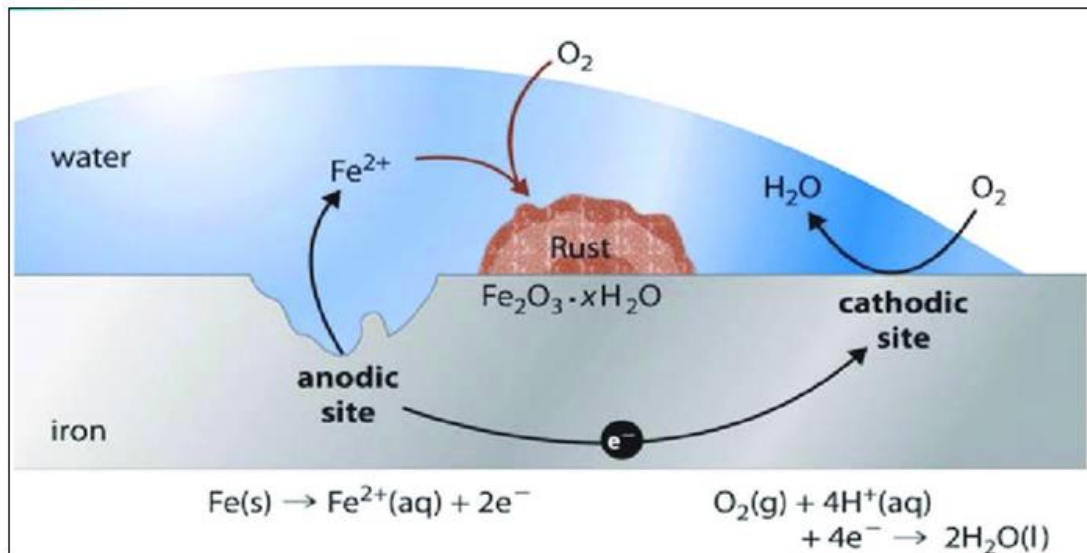


Figure 2.5: Corrosion half-cell reactions (Salunkhe and Rane, 2016)

The reaction of the anode includes the corroding of the anode metal, which goes into the electrolyte solution as metal ions. If we consider mild steel (mainly iron) for the anode reaction:



The cathode reaction consumes the electrons produced at the anode. If not, the anode becomes so charged with electrons so that all the reactions cease immediately. Otherwise, at the cathode, some reducible species in the electrolyte become adsorbed and pick up electrons to be reduced in a reduction process, although the cathode itself does not react (Bradford and Bradford 1993). Since the corrosive medium reacts at the cathode, several cathode reactions are possible, and different corrosives may attack metals. All environments are corrosive to some extent, and these include natural, urban, marine, and industrial atmosphere; fresh, distilled, salt and marine water; air and humidity; soil, bases, and acids (Zaki, 2006). The most popular reaction occurs in nature and neutral or alkaline solutions with dissolved oxygen (Bradford and Bradford 1993). That is:



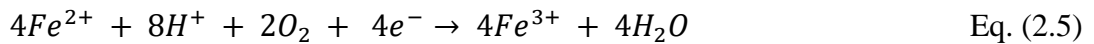
But in acidic solution (de-aerated), the cathodic reaction is:



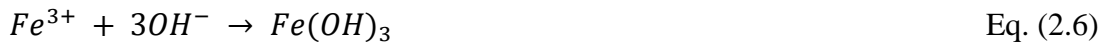
If no further oxidation or reduction reaction occurs, the overall corrosion reaction will be the combination of the anode and cathode half-cell reactions, which gives an insoluble iron (II) hydroxide known as green rust (Zaki, 2006). That is:



The iron (II) ions, which are usually unstable, may be further oxidized to stable iron (III) ions,



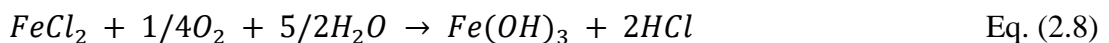
The iron (III) ions react with hydroxide ions to give hydrated iron (III) hydroxide, which is the common reddish-brown rust (ferric hydroxide).



When iron contacts with a hydrochloric acid solution, only ferrous chloride salt, and hydrogen gas can be detected,



The ferrous chloride could also be oxidized to ferric hydroxide,



Moreover, with aging, ferric hydroxide dehydrates even in the presence of water to give oxyhydroxides.



Oxidation and hydrolysis of ferric hydroxide may lead to the formation of all kinds of corrosion products, which include lepidocrocites ( $\gamma$ -FeOOH), goethite ( $\alpha$ -FeOOH), akaganite ( $\beta$ -FeOOH) and magnetite ( $Fe_3O_4$ ) and so on (Tamura, 2008).

## 2.6 Consequences of corrosion

Generally, the progression of corrosion shortens the life span of any metallic structure and this leads to structural deterioration, leakage, product degradation and environmental pollution. The corrosion problem in oil field applications, accounts for a significant proportion of the overall costs for oil and gas generating companies globally each year (Finšgar and Jackson, 2014). It occurs at all stages, from downhole to surface equipment and processing facilities, leading to serious problems, such as loss of life, adverse social effects, contamination of water supplies and the environment. It can also occur as leaks in tanks, casting, tubing, pipelines, and other equipment. Corrosion issues are commonly associated with operational problems and maintenance of equipment, leading to a repeated partial and even complete shutdown of the process resulting in significant economic losses (Finšgar and Jackson, 2014).

In the past, several disastrous incidences have been reported because of corrosion failures. One example is the sewer explosion in April 1992 in Guadalajara, Mexico, which took the lives of over 200 people. (Popoola et al., 2013). The series of explosions, in addition to the deaths, destroyed 1,600 buildings and wounded 1,500 people. The explosion was discovered to be due to the installation of a water pipe by a contractor many years before the explosion that spilled water onto a fuel line below. In turn, the deterioration of the gasoline pipeline caused the gasoline to spill into the



sewer. Moreover, corrosion is linked to almost all pipeline failures due to their long-term service and exposure to the aggressive environment (Hou et al., 2016).

## **2.7 Economic cost of corrosion**

The economic cost of corrosion is projected to be in the range of 1% - 5% of developed countries' gross national product, which include countries like United States, United Kingdom, Japan, Australia, Kuwait, Germany, Finland, Sweden, India, and China (Gerhardus et al., 2016). In 2016, a NACE report found that the estimated global cost of corrosion is at \$2.5 trillion yearly, an equivalent of about 3.4 percent of the global GDP (McMahon et al., 2019). While in Malaysia alone, the cost of corrosion amounts to about RM6.7 billion, which accounts for RM 207.4 billion of the country's GDP (Saupi et al., 2015). But between 15% - 35% of global savings will be achieved if current available, corrosion mitigation practices are implemented (Gerhardus et al., 2016).

## **2.8 Electrochemical corrosion monitoring techniques**

Since corrosion is an electrochemical method, the electrochemical characteristics of the metal-electrolyte interface, including corrosion potential and corrosion density, may suggest the appropriate corrosion monitoring technique. (Sastri, 2011). In monitoring corrosion processes, methods including electrochemical impedance spectroscopy, potentiodynamic polarisation, and electrochemical noise are widely employed. Complementary techniques used to classify the protective film formed on the metal surface, are surface analyses, such as scanning electron microscope coupled with energy dispersive X-ray, X-ray diffraction spectroscopy, and water contact angle analysis.

### 2.8.1 Electrochemical impedance spectroscopy (EIS)

Electrochemical impedance spectroscopy, also known as AC impedance, is now a well-developed laboratory technique used at different alternating current excitation frequencies, to obtain the electrical impedance of the metal-electrolyte interface. (Schweitzer, 2007). Impedance measurements considers the effect sum of resistance, capacitance, and inductance. Also, AC impedance can characterize the corrosion interface more comprehensively. Accurate corrosion interface tests can be performed with high quality equipment in a lower conductivity solution or under high-resistivity coatings. (Britton, 1979). Impedance measurements have many advantages, including the use of chemical inhibitors and protective coatings to predict corrosion rates, characterize systems under study and evaluate the resistance of alloys in certain environments (Schweitzer, 2007). Electrochemical impedance dependence on frequency and is the complex-valued proportionality factor  $\Delta E/\Delta I$  between the applied potential (or current) and the response current (or potential) in an electrochemical cell (Groisman, 2010).

Resistance  $R$ , from the DC theory, is given by Ohm's law as,

$$E = IR \quad \text{Eq. (2.10)}$$

where  $I$  is the current (in amperes, A), and  $E$  is the potential (in volts, V). Using Ohm's law and applying a DC potential to a circuit, the resulting current can be measured and from which the resistance be calculated.

while from AC theory,

$$E = IR \quad \text{Eq. (2.11)}$$

Where  $Z$  is the impedance, the AC equivalent of resistance. Impedance magnitude contains elements of equivalent circuit such as capacitors and inductors. The opposition to the flow of AC is provided by capacitors and inductors, just as resistors produce the same effect for DC. AC currents and voltages are vector quantities. Impedance can be expressed as a whole number where the resistance is the real component and the combined capacitance and inductance, the imaginary component (Ahmad, 2006). The total impedance is given as,

$$Z_{total} = Z' + Z''j \quad \text{Eq. (2.12)}$$

where  $Z'$  is the real impedance,  $Z''$  is the imaginary impedance and  $j$  is  $\sqrt{-1}$ . The expression for the absolute magnitude of impedance will be:

$$|Z| = \sqrt{(Z')^2 + (Z'')^2} \quad \text{Eq. (2.13)}$$

and,

$$\tan \theta = Z'/Z'' \quad \text{Eq. (2.14)}$$

When the opposition to current flow is due to capacitive resistance, the current leads the applied voltage in phase angle. But when inductive reactance is responsible for the opposition to current flow, the current lags behind the voltage in phase angle (Ahmad, 2006). The phase angle ( $\theta$ ) or phase shift is the difference between points on the x-axis where current and voltage curve amplitudes are zero (Figure 2.6). The electrochemical impedance expressions based on circuit components are given in Table 2.1.

Table 2.1: Electric circuit components in electrochemical impedance

Circuit components	Impedance
Resistor, $R$	$Z = R$
Capacitor, $C$	$Z = -1/j\omega C$
Inductor, $L$	$Z = j\omega L$

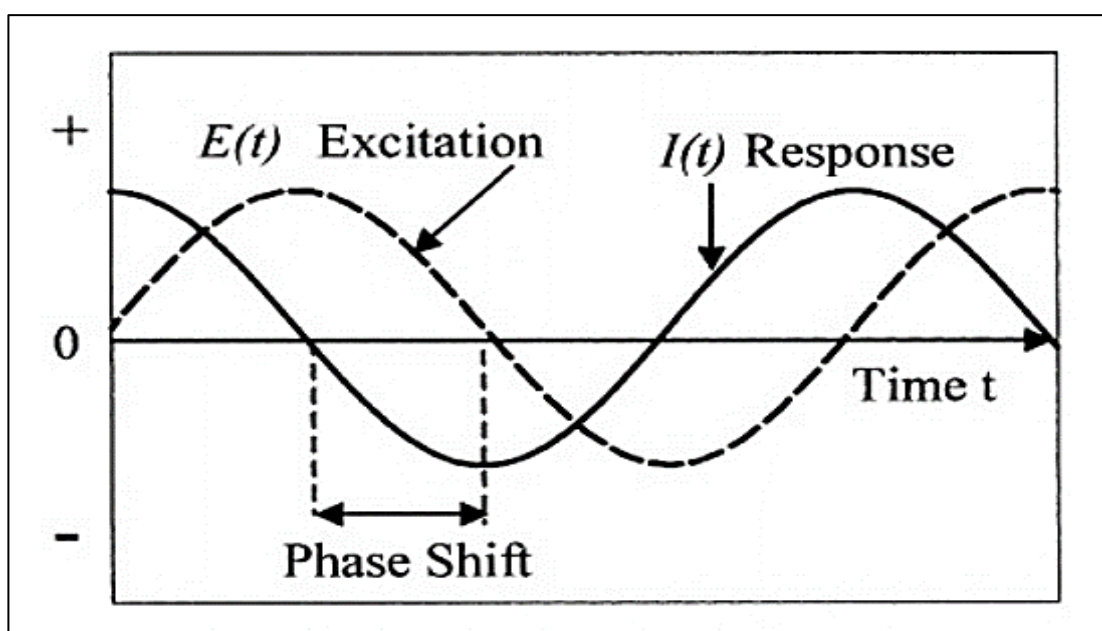


Figure 2.6: EIS potential excitation and current response (Perez, 2004)

Electrochemical impedance measurement produces numerical results that are presented in three (3) kinds of plots (Lasia, 2005): Nyquist plots, also called complex plane plots of imaginary  $Z''$  versus real impedance  $Z'$  (Figure 2.7). There are two types of Bode plots; Bode magnitude  $|Z|$  versus the logarithm of frequency  $\log \omega$  and phase angle  $\theta$  versus the logarithm of frequency  $\log \omega$  (Figure 2.8).

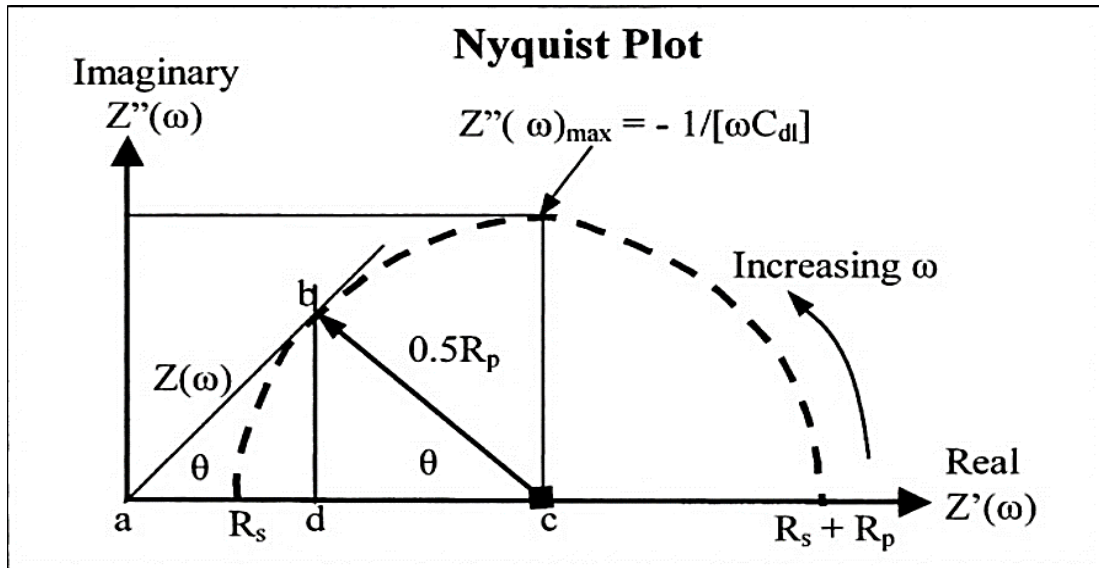


Figure 2.7: Nyquist plots (Perez, 2004)

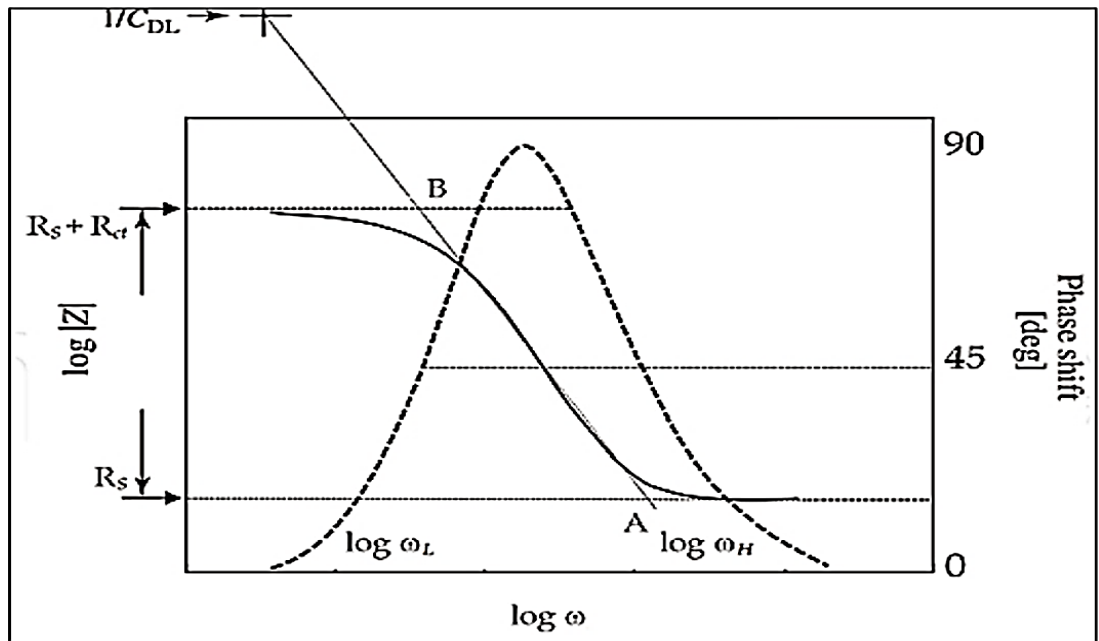


Figure 2.8: Bode plots (Berradja, 2019)

From these plots, corrosion resistance of metal or alloy under electrochemical impedance analysis can be accurately estimated. Usually, a well-known Randles equivalent circuit (RC circuit), which describes many electrochemical electrode-electrolyte characteristic interfaces, represents the impedance corresponding to a simple corrosion mechanism under activation control. A typical example of a Randle-

type equivalent circuit is depicted in Figure 2.9. For a charge-transfer control (Figure 2.9 a), only the solution resistance ( $R_s$ ), polarization resistance ( $R_p$ ), and capacitance  $C$ , corresponding to the double-layer capacitor ( $C_{dl}$ ), are required in a simple circuit. Thus, the impedance for this circuit becomes,

$$Z = R_s + R_p / 1 + j\omega C_{dl} R_p \quad \text{Eq. (2.15)}$$

The double layer capacitance can be gotten from the expression,

$$C_{dl} = 1 / 2\pi f_{max} \times 1 / R_p \quad \text{Eq. (2.16)}$$

Where  $f_{max}$  is the frequency at which the imaginary component of the Nyquist plot is maximum.

In corrosion inhibition study, an increase in the polarization resistance and decrease in the double layer capacitance with increasing inhibitor concentration indicate that the inhibitor compound (s) inhibit the metal's corrosion rate via charge transfer mechanism (Perez, 2004). But when the electrochemical system is diffusion-controlled (Figure 2.9 b), a diffusion impedance ( $Z_D$ ) known as Warburg impedance is introduced in the circuit.

For a coating system, the use of a different equivalent circuit containing parallel arrangement of resistors and capacitors with coating resistance  $R_{coat}$  and coating capacitive element  $CPE_{coat}$  as additional circuit components is employed.

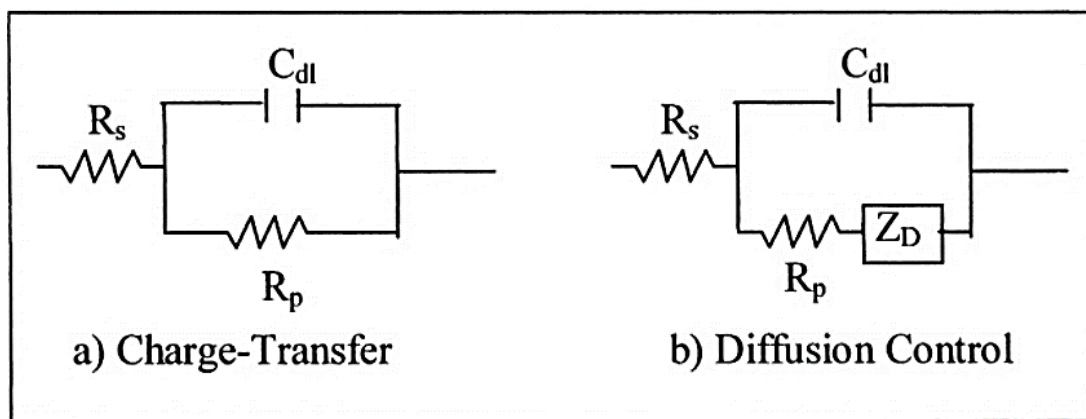


Figure 2.9: Common electrochemical circuits used in corrosion studies (Perez, 2004)

### 2.8.2 Potentiodynamic polarization (PD)

This is mainly a popular electrochemical laboratory technique used to study corrosion phenomena, particularly pitting, (Britton, 1979). The working electrode, which acts as the sensing part, is typically polarised using a three-electrode corrosion probe. The current response is measured as potential is varied from the free-corrosion potential. This technique is useful in estimating the anodic and cathodic Tafel slopes. The polarisation technique includes the use of mathematical models to describe the kinetics of charge transfer process in an electrochemical environment, according to Perez (2004). The electrode reactions are presumed to induce equilibrium deviations because of the flow of electric current through an electrochemical cell, which causes a change in the potential of the working electrode (WE). Consequently, a difference between the electrical potential of the polarized and unpolarized (equilibrium) electrode potential, known as the overpotential ( $\eta$ ) is produced. The electrochemical and chemical reaction rates due to anodic or cathodic overpotentials can usually be predicted with the respective equations of Faraday (Eq. 2.17) and Arrhenius (Eq. 2.18) (Perez, 2004),

$$R_F = iA_{wj}/zF \quad \text{Eq. (2.17)}$$

$$R_A = \gamma_a \exp(-\Delta G^*/RT) \quad \text{Eq. (2.18)}$$

For where  $i$  is the applied current density ( $\text{A cm}^{-2}$ ),  $A_{wj}$  is the atomic weight of species  $j$  ( $\text{g mol}^{-1}$ ),  $z$  is the state of oxidation or number of valency,  $\gamma_a$  is the chemical reaction constant, and  $\Delta G^*$  is the activation energy or free energy change ( $\text{J mol}^{-1}$ ).

At equilibrium, Faraday's equation equals Arrhenius rate equation ( $R_F = R_A$ ) then, the current density becomes,

$$i = \gamma_a \exp(-\Delta G^*/RT) \quad \text{Eq. (2.19)}$$

Otherwise, if an overpotential polarizes an electrode under steady-state conditions, the reaction rates will not be equal ( $R_F \neq R_A$ ). Hence, the forward ( $i_f$  cathodic) and reverse ( $i_r$  anodic) current densities components will have to be defined in terms of free energy change  $\Delta G$ , as deduced from Figure 2.10, where  $k'_f$  and  $k'_r$  is the forward and reverse reaction rates, respectively. Thus,

$$i_f = k'_f \exp(-\Delta G_r^*/RT) \text{ (cathodic)} \quad \text{Eq. (2.20)}$$

$$i_r = k'_r \exp(-\Delta G_f^*/RT) \text{ (anodic)} \quad \text{Eq. (2.21)}$$

and,

$$\Delta G_f^* = \Delta G_f - \alpha z F \eta_c \quad \text{Eq. (2.22)}$$

$$\Delta G_r^* = \Delta G_r + (1 - \alpha) z F \eta_a \quad \text{Eq. (2.23)}$$



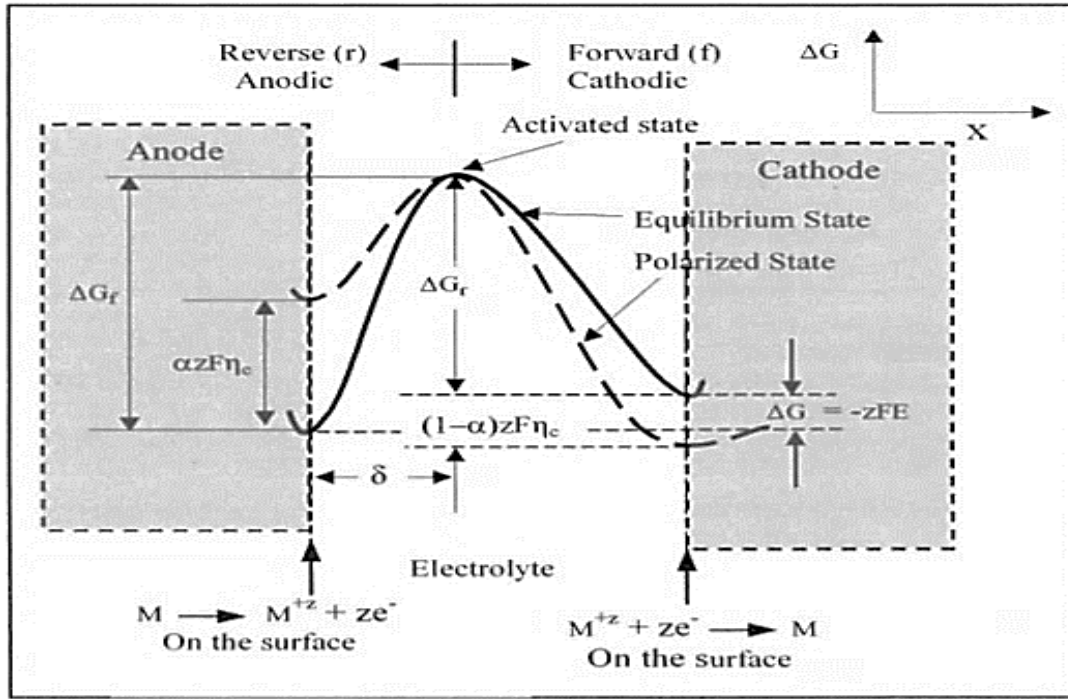


Figure 2.10: Schematic activation free energy distribution (Perez, 2004)

Where  $\alpha$  is the symmetry coefficient,  $F$  is the Faraday's constant, and  $\eta$  is the overpotential reaction or polarization for both anodic and cathodic reactions. In the cathodic case, the net current is  $i = i_f - i_r$  and the overpotential is  $\eta_c$ . The net current density is given in a general form by substituting equations (2.20) and (2.21) into this expression gives. That is,

$$i = k'_f \exp(-G_f^*/RT) \exp(\alpha ZF\eta/RT) - k'_r \exp(-\Delta G_r^*/RT) \exp(-(1-\alpha)zF\eta/RT) \quad \text{Eq. 2.24}$$

From this equation (2.24), the exchange current density is deduced as:

$$i_o = k'_f \exp(-\Delta G_f^*/RT) = k'_r \exp(-\Delta G_r^*/RT) \quad \text{Eq. (2.25)}$$